Nanoscale Advances

ROYAL SOCIETY OF CHEMISTRY

PAPER

View Article Online
View Journal | View Issue

Cite this: *Nanoscale Adv.*, 2023, **5**, 4133

V-doped porous CoP nanoarrays grown on carbon cloth with optimized electronic structure for the hydrogen evolution reaction†

Wenzhi Jia, ‡[a] Qian Lu,‡[a] Wenjun Zheng,[a] Kunyan Wang,[a] Xinhua Liu,[b] Shichun Yang[b] and Bin He *[a]

Received 22nd May 2023
Accepted 7th July 2023

DOI: 10.1039/d3na00348e

rsc.li/nanoscale-advances

As an efficient, renewable and clean energy, hydrogen is expected to replace traditional fossil fuel energy in the future. Currently, platinum-based materials (Pt) are excellent electrocatalysts for hydrogen evolution reaction (HER), but their high cost and low natural abundance limit their widespread application. Therefore, it is urgent to develop low-cost, highly efficient and earth-abundant electrocatalysts to replace the precious platinum-based materials. In this study, a Co-based organic framework (ZIF-67) was grown on a flexible substrate carbon cloth (CC), and a V-doped CoP nanoarray (V-CoP/CC) was prepared using a simple *in situ* ion exchange/phosphating method. Due to its unique porous structure, effective doping of V atoms and the *in situ* electrode construction, the V-CoP/CC exhibited high electrolytic hydrogen evolution reaction (HER) performance, with an overpotential of 98 mV at a current density of 10 mA cm^{-2}. This work has important theoretical and practical significance for *in situ* construction of heteroatom-doped CoP electrodes.

1 Introduction

In recent years, the rapid consumption of fossil fuels and environmental pollution has seriously hindered human survival and development. Developing efficient and renewable clean energy is now a top priority.[1,2] Hydrogen (H_2) produced through electrochemical methods is considered a clean, efficient, and sustainable alternative to fossil fuels, and is expected to alleviate the problems caused by the energy crisis.[3] As is well known, platinum-based materials have been regarded as the most state-of-the-art electrocatalysts for hydrogen evolution reactions (HER). However, the natural scarcity and high cost of Pt-based materials limit their large-scale production and utilization. Therefore, it is urgent to explore and develop efficient and resource-rich non-precious metal electrocatalysts to replace Pt-based materials.

Earth-abundant transitional metal-based catalysts have shown high electrocatalytic performance in HER reaction, with the potential to replace precious metal catalysts.[4] In particular, transition metal phosphides (TMPs) have attracted extensive attention due to their adjustable electronic structure, high electrocatalytic activity, low cost, and similarity to hydrogenase. However, most TMP electrocatalysts only exhibit high activity in an alkaline or acidic medium and still require very high overpotentials to drive HER, especially in neutral electrolytes.[5,6] Additionally, TMPs are often limited by low active site density, poor stability, and slow reaction kinetics.[7] To improve the catalytic activity of TMPs, the main strategies are as follows: (i) morphological structure regulation of the catalyst to improve the specific surface area and increase the active site. Metal–organic frameworks (MOFs) are a new type of porous material that can be used as excellent template precursors for the design and synthesis of corresponding phosphide derivatives.[8] For instance, Wang *et al.* reported that MOFs,[9] as a template and precursor, formed bimetallic phosphide with a heterogeneous structure and improved the intrinsic active site of the catalyst. The hollow 3D framework of Co–Fe bimetallic phosphide prepared by the MOFs precursor is an excellent catalyst for electrochemical water decomposition.[10] Therefore, MOFs can be used to construct effective geometric structures for electrocatalytic reactions. (ii) Regulating the electronic structure of the catalyst to optimize the intermediate adsorption energy in the reaction process and improve the electron transport ability to enhance the activity of the catalyst.[11] Among them, atomic doping is an effective route to regulate the electronic structure of catalysts. For example, Zhou *et al.* reported that regulating the electronic structure of TMPs by heteroatom doping is a powerful strategy that can further enhance its intrinsic activity.[12] Effective doping of materials can improve the electrocatalytic efficiency.

[a]*Department of Materials Engineering, Huzhou University, Huzhou 313000, China. E-mail: binhe@zjhu.edu.cn*

[b]*School of Transportation Science and Engineering, Beihang University, Beijing, 100191, China*

† Electronic supplementary information (ESI) available. See DOI: https://doi.org/10.1039/d3na00348e

‡ These authors contributed equally to this work.

In this paper, a Co-based organic framework (ZIF-67) was grown on a flexible carbon cloth (CC) substrate, and V-doped CoP nanoarray (V-CoP/CC) was prepared using a simple *in situ* ion exchange/phosphating method. The optimized electronic structure of V-doped CoP is achieved by the introduction of V dopants, which can enhance the charge transfer and improve the HER activity. The V-doped CoP nanoarrays are characterized by SEM, XRD, TEM and XPS. By constructing *in situ*, three-dimensional porous nanosheet structures and doping V ions, V-CoP/CC exhibited excellent HER electrocatalytic activity, with an overpotential of 98 mV at a current density of 10 mA cm^{-2}. This work provides a simple strategy for constructing three-dimensional porous heteroatom-doped metal phosphating materials.

2 Experimental

2.1. Synthesis of Co-MOF/CC

First, the carbon cloth was treated with 6 mol L^{-1} nitric acid at 85 °C for 12 h. 0.65 g $Co(NO_3)_2 \cdot 6H_2O$ was dissolved in 50 mL deionized water, and the solution A was formed after ultrasound for 15 min. 1.46 g 2-methylimidazole was dissolved in 50 mL deionized water and ultrasonic for 15 min to form solution B. Then, pour solution B into solution A and stir ultrasonic for 15 min. Subsequently, the treated carbon cloth (2 × 5 cm^2) was immersed in the above mixed solution and reacted at room temperature for 4 h. The final product was washed 3 times in water and ethanol and dried in an oven at 40 °C for 8 h.

2.2. Synthesis of V-CoP/CC

A piece of Co-MOF/CC (2 × 2.5 cm^2) was put into an ethanol/water solution (1 : 4, 50 mL), containing 10 mg Na_3VO_4, and the Co-MOF/CC was converted to V-$Co(OH)_2$/CC after reflux reaction at 85 °C for 15 min. Then, V-$Co(OH)_2$/CC (2 × 2.5 cm^2) and 300 mg NaH_2PO_2 were placed in the tubular furnace, respectively. NaH_2PO_2 was located in the upstream of N_2 gas flow, and the heating rate was 2 °C min^{-1}, and the reaction was conducted at 350 °C for 2 h. The mass loading amount of V-CoP/CC on CC is 1.9 mg cm^{-2}.

2.3. Synthesis of CoP/CC

Co-MOF/CC (2 × 2.5 cm^2) was put into an ethanol/water solution (1 : 4, 50 mL) containing 10 mg $Co(NO_3)_2 \cdot 6H_2O$. Co-MOF/CC was converted to $Co(OH)_2$/CC after reflux reaction at 85 °C for 15 min. Then, $Co(OH)_2$/CC (2 × 2.5 cm^2) and 300 mg NaH_2PO_2 were placed in a tubular furnace, with NaH_2PO_2 located in the upstream of N_2 gas flow. The heating rate was 2 °C min^{-1}, and the reaction was conducted at 350 °C for 2 h.

2.4. Synthesis of Pt/C/CC

Pt/C/CC was prepared according to the method reported in previous literature,[13] 5 mg Pt/C was dispersed evenly in Nafion isopropyl alcohol solution (180 μL isopropyl alcohol and 20 μL Nafion) to form a uniform mixture. The suspension was then loaded on 1 × 1 cm^2 CC and dried at 40 °C for 8 h.

2.5. Characterization

Powder X-ray diffraction (XRD) was performed on a Model D/max-rC X-ray diffractometer with Cu target Kα lines. The surface morphology and microstructure of the prepared samples were analyzed by scanning electron microscopy (SEM, Hitachi S-4800 scanning) and transmission electron microscopy (TEM, JEOL JEM-2010F). X-ray photoelectron spectroscopy (XPS) of the samples was analyzed by Thermo ESCALAB 250 test.

2.6. Electrochemical performance test

All experimental electrochemical tests were performed at the CHI 660 electrochemical workstation, using carbon cloth, carbon rod and saturated calomel electrodes for growing catalysts as working, opposite and reference electrodes, respectively, in a typical three-electrode system. With 1.0 M KOH solution as the electrolyte, the electrolyte before the HER test was aerated with N_2 for 30 min. Linear sweep voltammetry (LSV) has a sweep rate of 5 mV s^{-1}, corrected by infrared compensation. Potential reference reversible hydrogen electrode (RHE): $E_{RHE} = E_{SCE} + 0.0591\ pH + 0.242$. Overpotential ($\eta$) calculation is as follows: $\eta = E$ (*vs.* RHE) 1.23. The frequency range of electrochemical impedance spectroscopy (EIS) is 0.01 Hz to 100 kHz, and the amplitude of the test is 5 mV.

3 Results and discussion

3.1 Preparation and characterization of V-CoP/CC

The synthesis process of the V-CoP/CC nanosheet array is shown in Fig. 1. Co-MOF/CC nanosheet arrays were prepared on CC cloth by co-precipitation method with $Co(NO_3)_2 \cdot 6H_2O$ and 2-methylimidazole aqueous solution as main raw materials. Co-MOF grew uniformly and vertically on the CC surface. SEM images showed that Co-MOF was in the shape of a three-dimensional blade (Fig. S1†), with a smooth surface and a thickness of about 100 nm. The XRD results (Fig. S2†) show that the diffraction peaks at 25.5 and 43.5° are attributed to carbon cloth, and the XRD peaks after Co-MOFs grow on the surface are consistent with previous literature, indicating that the synthesis of Co-MOF/CC is successful.[14]

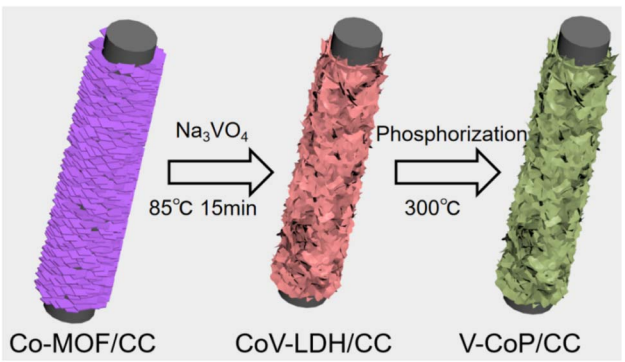

Fig. 1 Schematic diagram of the preparation process of V-CoP/CC catalyst.

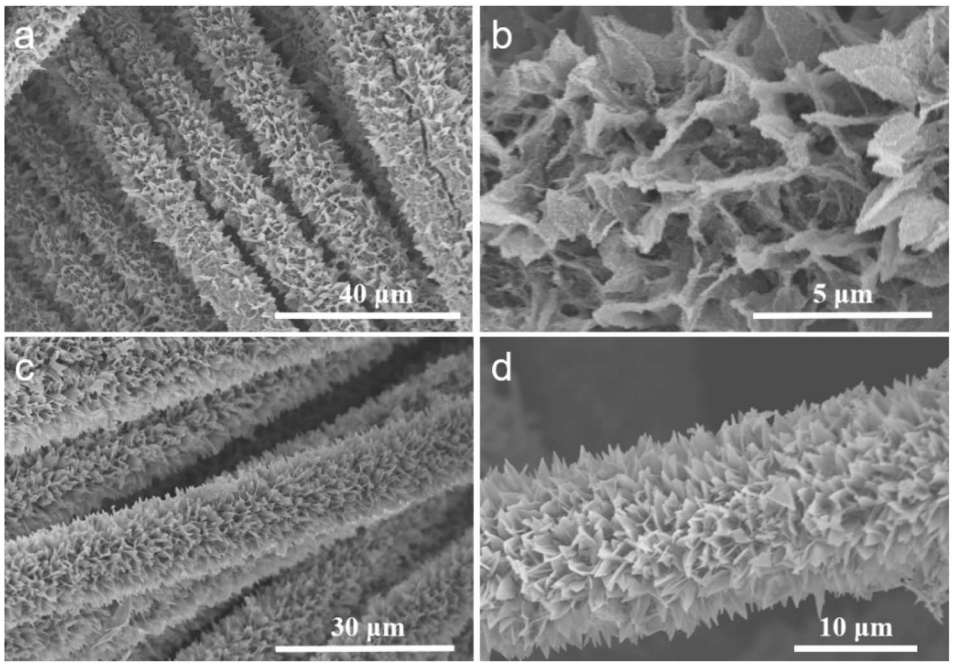

Fig. 2 SEM diagram of V-doped $Co(OH)_2$ (LDH) (a–d).

Subsequently, Co-MOF/CC is converted to V-Co-LDH/CC by ion exchange. Due to the hydrolysis of Co-MOF, the released Co^{2+} is ion exchanged with OH^- and VO_4^{3-} to form V-Co layered bi-hydride (V-Co LDH) on the surface.[15,16] As seen from the SEM results, the V-$Co(OH)_2$/CC catalyst presents a three-dimensional lamellar structure with a large number of nanosheets attached to the surface (Fig. 2). Besides, the weak X-ray diffraction peak of V-$Co(OH)_2$/CC is consistent with the standard JCPDS (no. 51-1731) assigned to $Co(OH)_2$, further confirming the successful conversion of Co-MOF to V-$Co(OH)_2$ on the carbon cloth (Fig. S3†).

After the phosphating process at 350 °C under an N_2 atmosphere, the morphology changes of V-CoP/CC, as shown in Fig. 3. SEM results show that the originally smooth nanosheet array (Fig. 3a and b) becomes rough and porous (Fig. 3c and d). Fig. 6 shows the V-CoP/CC vertical nanochannel array after

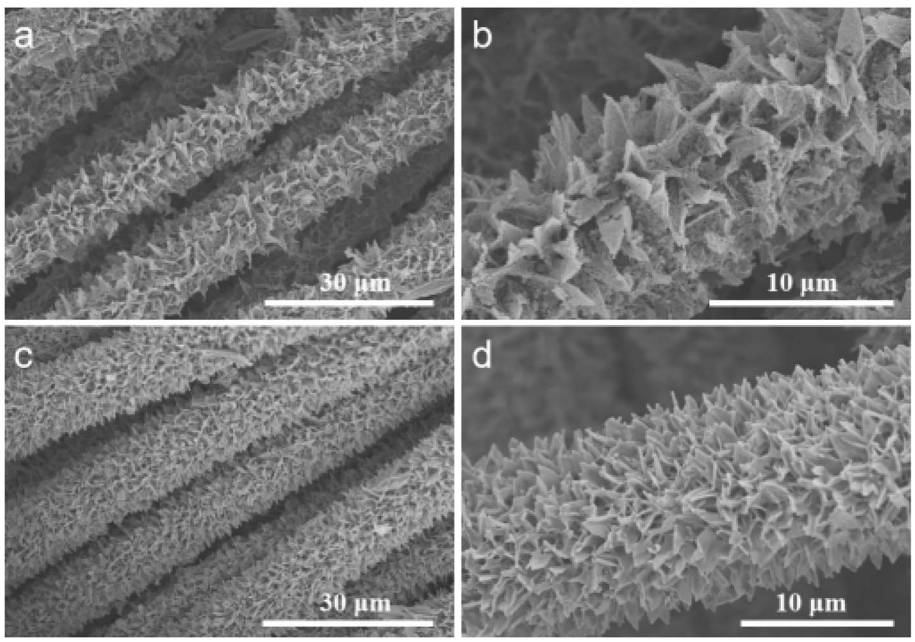

Fig. 3 (a)–(d) SEM images of V-CoP/CC.

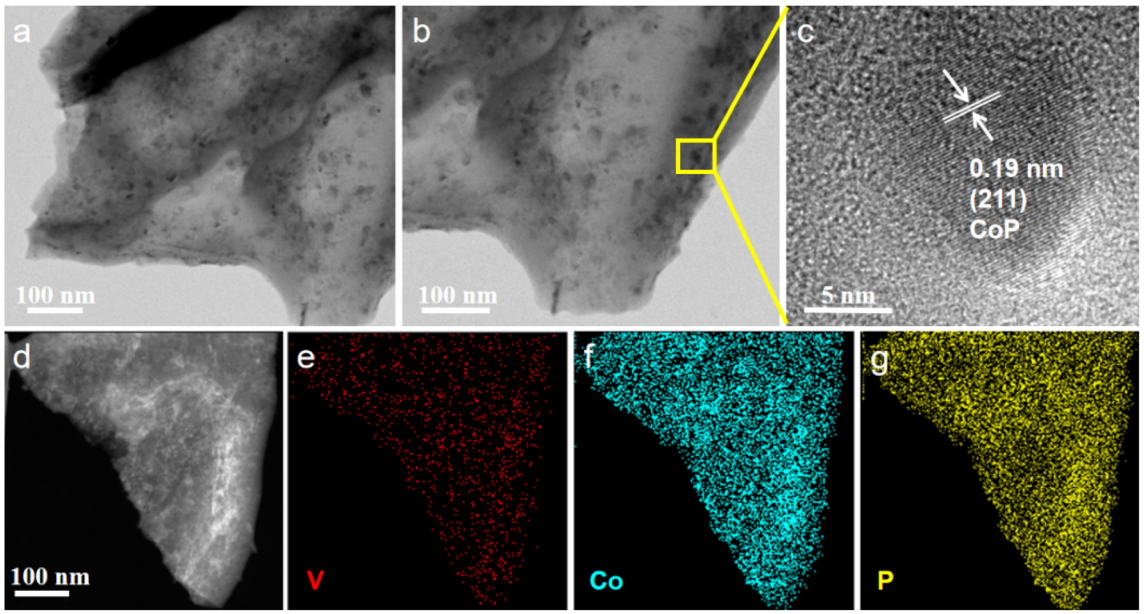

Fig. 4 (a) and (b) TEM, (c) HRTEM and (d)–(g) EDS elements of V-CoP@C.

phosphating without collapse and aggregation, indicating a firm contact between V-CoP and CC cloth. Vertically aligned CoP nanoarrays with three-dimensional open frames can not only maximize the exposed reaction sites, but also greatly promote the acquisition of electrolytes and the release of hydrogen during the HER process, thus significantly improving HER catalytic performance.[17] Fig. S4† shows the XRD pattern of the prepared V-COP/CC catalyst. The results show that all

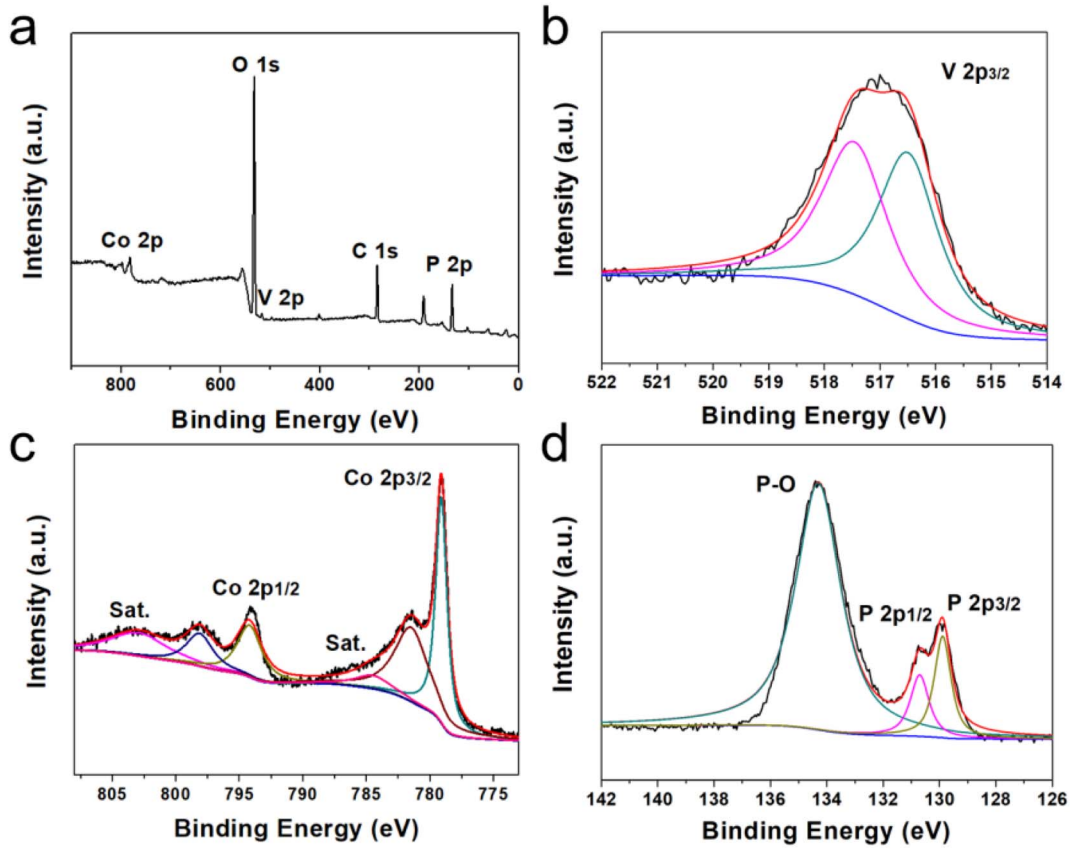

Fig. 5 (a) Full XPS spectrum of V-CoP@C and high resolution spectra of (b)–(d) V 2p, Co 2p and P 2p.

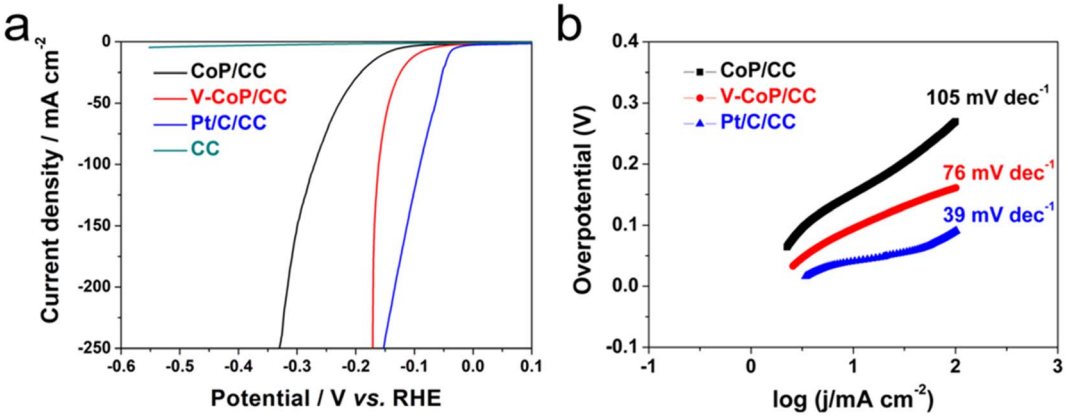

Fig. 6 (a) Polarization curve, (b) Tafel slope.

diffraction peaks, except the carbon cloth peak, belong to CoP (JCPDS: 65-1474), and no diffraction peaks of V-based compounds are found, indicating that V atoms are doped into the CoP lattice during phosphating.

The morphology and element distribution of V-CoP/CC were characterized by transmission electron microscopy (TEM), high-resolution transmission electron microscopy (HRTEM) and energy dispersion spectrometer (EDS), as shown in Fig. 8. TEM images confirmed that the surface of the V-CoP nanosheet array was composed of nanoparticles (Fig. 4a), which was consistent with SEM results. According to HRTEM results (Fig. 4c), the lattice spacing of the V-CoP is 0.19 nm, attributed to the CoP (211) plane. Additionally, the HAADF-STEM image of V-CoP and the corresponding EDS element mapping image are shown in Fig. 4e–g. It can be seen that the elements V, Co and P are evenly distributed on the entire surface of the V-CoP sample, indicating that the element V is uniformly doped on the CoP.

The surface chemical composition of V-CoP/CC was analyzed by X-ray photoelectron spectroscopy (XPS). As shown in Fig. 5a, the XPS spectrum of the prepared sample shows the presence of elements V, Co and P. Fitting the V 2p peaks (Fig. 5b), the peaks at the binding energies (Bes) of 516.5 and 517.5 eV are attributed to V^{4+} and V^{5+}, respectively, suggesting that V species exist in the lattice of V-CoP/CC as V^{4+} and V^{5+}.[18] In the Co 2p XPS spectrum (Fig. 5c), there are two peaks at 784.6 and 803.1 eV with a satellite peak, among which the spin orbit twin peaks at 779.1 and 794.3 eV are attributed to the Co–P bond.[19] The spin orbit twin peaks at 781.6 and 798.3 eV correspond to the CoO_x.[20] The high-resolution P 2p spectrum has three main peaks from the P $2p_{3/2}$, P $2p_{1/2}$ and P–O bonds at 129.9, 130.7 and 134.3 eV, respectively (Fig. 5d).

3.2 Electrocatalytic hydrogen evolution performance of V-CoP@C

The electrocatalytic properties of Pt/C/CC, CoP/CC and V-CoP/CC in 1.0 M KOH solution were recorded using a three-electrode system. Fig. 6a shows that at a current density of 10 mA cm^{-2}, the overpotential of the Pt/C/CC catalyst is 39 mV, indicating the best HER reaction activity. The overpotential of V-CoP/CC at a current density of 10 mA cm^{-2} is only 98 mV, which is much lower than the catalytic performance of CoP (149 mV). This indicates that V doping plays a key role in improving the performance of the CoP catalyst. The HER performance of V-CoP/CC was much more optimal than the other Co-based catalysts from the recent literature (Table S1†and Fig. 7). To evaluate HER kinetics, the Tafel slopes of the three catalysts were tested, and the results are shown in Fig. 6b. As can be seen from these results, the slope values of CoP/CC, V-CoP/CC and Pt/C/CC catalysts are 105 mV dec^{-1}, 76 mV dec^{-1} and 39 mV dec^{-1}, respectively. The comparison shows that V-CoP/CC has better reaction kinetics and faster charge transfer than CoP/CC in alkaline electrolytes.

Fig. S5† shows the cyclic voltammetry (CV) of CoP/CC and V-CoP/CC. The double-layer capacitance (C_{dl}) was also evaluated using electrochemically active surface area (ECSA) (Fig. 8). The V-CoP/CC catalyst was observed to have a higher electrochemical surface area than the CoP/CC catalyst at different sweep voltammetry of 20–100 mV s^{-1}(scan rate: 20, 40, 60, 80, 100 mV s^{-1}) at the potential range of 0.06–0.2 V.[21–24] The C_{dl} value of the V-CoP/CC electrode was 7.73 mF cm^{-2}, which was much higher than that of CoP/CC (6.53 mF cm^{-2}), indicating

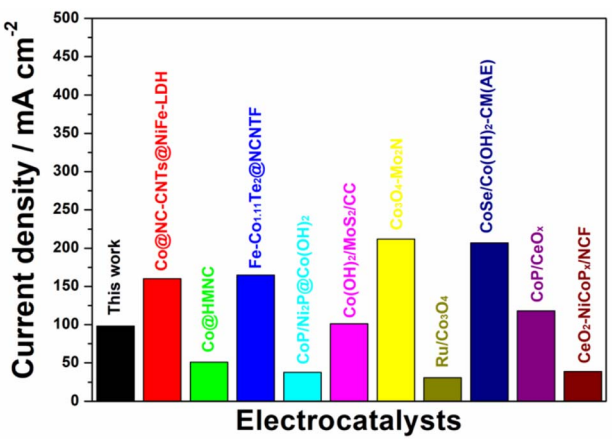

Fig. 7 Overpotential (η_{10}) comparison plot of Co-based catalysts based recent literature.

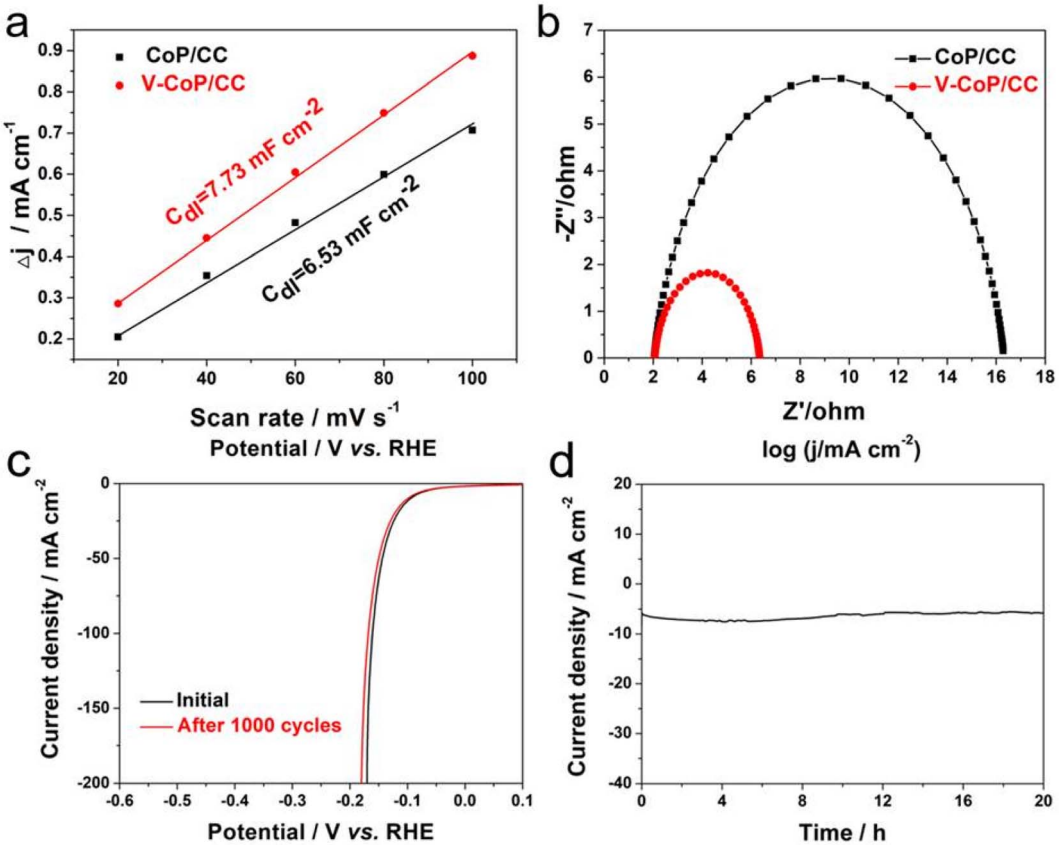

Fig. 8 (a) Values of the electrochemical double layer capacitance (C_{dl}) of CoP/CC and V-CoP/CC, (b) Nyquist curve, (c) polarization curves of V-CoP/CC initially and after 1000 CV cycles, (d) time-dependent current density curves.

that more active sites were exposed on the catalysts surface during the reaction. This further indicated that V-doping promotes electrolyte acquisition and H_2 gas release in the HER process, significantly improving HER catalytic performance. The comparison of the Nyquist plots of the catalyst confirmed that the interfacial electron transfer resistance (R_{ct}) of V-CoP/CC was less than that of CoP/CC (Fig. 8b). These results demonstrate that the V-CoP/CC catalyst has the highest conductivity and the fastest interfacial electron transfer during the alkaline HER process.[25,26]

Electrochemical stability is another important factor in evaluating the excellent performance of HER electrocatalysts.[27,28] In a 1.0 M KOH solution, the V-CoP/CC catalyst underwent a 1000 CV cycles test and chrono-current performance test. The stability test results are shown in Fig. 8c and d. The LSV curve after 1000 CV cycles was well overlapped with the initial one, and the performance attenuation of the V-CoP/CC catalyst was negligible compared to the first cycle of 1000 consecutive CV tests, indicating its superior stability in alkaline conditions. The SEM images reveal that the V-CoP/CC catalyst maintained its rough and porous morphology after stability testing, demonstrating good structural stability of the catalyst (Fig. S6a†). Furthermore, XRD pattern of the V-CoP/CC catalyst after stability testing was consistent with the pattern of CoP, indicating that the crystalline structure was maintained during the stability testing (Fig. S6b†). In addition, the V-CoP/CC catalyst showed good stability after continuous electrolysis for 20 h (Fig. 8d), with little increase in potential. In summary, the results demonstrate that the V-CoP/CC catalyst has good long-term stability for HER in an alkaline solution.

4 Conclusion

In this study, the Co-foundation organic framework (ZIF-67) was grown on a flexible carbon cloth (CC), followed by prepared V-doped CoP nanosheet array (V-CoP/CC) using a simple *in situ* ion exchange/phosphating method. This method allowed for the *in situ* generation of V-CoP/CC on a CC cloth with high conductivity, eliminating the need for separate synthesis. Scanning electron microscopy (SEM) results showed that the V-CoP/CC surface had a rough three-dimensional blade-like structure, which increased the electrochemical surface area, facilitated faster electron transport, and exposed more catalytic active sites. Additionally, doping V ions promoted electrolyte acquisition and H_2 gas release during the HER process, while the synergistic effect of V and Co atoms further improves HER performance. The three-dimensional blade structure of the V-CoP/CC catalyst demonstrated high reaction stability for HER in an alkaline solution, with an overpotential of 98 mV at a current density of 10 mA cm^{-2}. This work provides a new

strategy for the development of Pt-based non-noble metal electrocatalysts.

Conflicts of interest

There are no conflicts to declare.

Acknowledgements

This work was financially supported by the National Natural Science Foundation of China (No. 21603069), Students innovation and entrepreneurship training program of Huzhou University (202201253), Start-up funding for talent research in 2022 (RK33047), the Public Welfare Application Research Project of Huzhou City (grant numbers 2021GZ09).

References

1 X. Y. Zhao, B. L. He, J. Zhang, C. F. Du, Q. Ye and S. J. Liu, *Vacuum*, 2022, **198**, 110888.
2 L. Sun, T. Wang, L. Zhang, Y. J. Sun, K. W. Xu, Z. F. Dai and F. Ma, *J. Power Sources*, 2018, **377**, 142–150.
3 X. C. Du, J. W. Huang, J. J. Zhang, Y. C. Yan, C. Y. Wu, Y. Hu, C. Y. Yan, T. Y. Lei, W. Chen, C. Fan and J. Xiong, *Angew. Chem., Int. Ed.*, 2019, **58**, 4484–4502.
4 R. L. Zhu, F. F. Chen, J. Y. Wang, Y. Y. Song, J. L. Cheng, M. Mao, H. J. Ma, J. J. Lu and Y. L. Cheng, *Nanoscale*, 2020, **12**, 9144–9151.
5 G. Zhang, B. Wang, J. Bi, D. Fang and S. Yang, *J. Mater. Chem. A*, 2019, **7**, 5769–5778.
6 Y. Zheng, Y. Jiao, A. Vasileff and S. Z. Qiao, *Angew. Chem., Int. Ed.*, 2017, **57**, 7568–7579.
7 X. Wang, Z. J. Ma, L. L. Chai, L. Q. Xu, Z. Y. Zhu, Y. Hu, J. J. Qian and S. M. Huang, *Carbon*, 2019, **141**, 643–651.
8 H. Furukawa, K. E. Cordova, M. O'Keeffe and O. M. Yaghi, *Science*, 2013, **341**, 1230444.
9 L. Wang, N. Gong, Z. Zhou, Q. C. Zhang, W. C. Peng, Y. Li and F. B. Zhang, *Chin. J. Catal.*, 2022, **43**, 1176–1183.
10 Y. Lian, H. Sun, X. Wang, P. Qi, Q. Mu, Y. Chen, J. Ye, X. Zhao, Z. Deng and Y. Peng, *Chem. Sci.*, 2019, **10**, 464–474.
11 Y. Pan, K. Sun, Y. Lin, X. Cao, Y. S. Cheng, S. J Liu, L. Y. Zeng, W. C. Cheong, D. Zhao, K. L. Wu, Z. Liu, Y. Q. Liu, D. S. Wang, Q. Peng, C. Chen and Y. D. Li, *Nano Energy*, 2019, **56**, 411–419.
12 J. Q. Zhou, Y. L. Xie, L. Yang, Y. S. Liu, Y. Du, L. Yu and Y. Yu, *Inorg. Chem. Front.*, 2023, **10**, 2842–2859.
13 Z. Zhang, X. Ma and J. Tang, *J. Mater. Chem. A*, 2018, **6**, 12361–12369.
14 M. Sun, Q. Ye, L. Lin, Y. F. Wang, Z. M. Zheng, F. F. Chen and Y. L. Cheng, *J. Colloid Interface Sci.*, 2023, **637**, 262–270.
15 J. T. Zhang, H. Hu, Z. Li and X. W. Lou, *Angew. Chem., Int. Ed.*, 2016, **128**, 4050–4054.
16 X. H. Du, Y. N. Fang, J. B. Guan, S. S. Li, L. N. Wang and M. Zhang, *Int. J. Hydrogen Energy*, 2021, **46**, 599–608.
17 L. Y. Zeng, K. A. Sun, X. B. Wang, Y. Q. Liu, Y. Pan, Z. Liu, D. W. Cao, Y. Song, S. H. Liu and C. G. Liu, *Nano Energy*, 2018, **51**, 26–36.
18 Y. F. Cheng, F. Liao, W. Shen, L. B. Liu, B. B. Jiang, Y. Q. Li and M. W. Shao, *Nanoscale*, 2017, **9**, 18977.
19 S. B. Guo, W. B. Zhang, Z. Q. Yang, S. S. Chai, X. L. Zhang, X. Zhou, X. W. Han and J. P. Long, *J. Alloys Compd.*, 2023, **944**, 169160.
20 C. Xu, Y. Q. Jiang, J. H. Yang, W. M. Wu, X. Qian and L. X. Hou, *Chem. Eng. J.*, 2018, **343**, 86–94.
21 Y. F. Cheng, F. Liao, W. Shen, L. B. Liu, B. B. Jiang, Y. Q. Li and M. W. Shao, *Nanoscale*, 2017, **9**, 18977–18982.
22 Y. R. Ren, P. C. Ye, J. D. Chen, H. Y. Wang, J. Q. Ning, J. L. Shen, Y. J. Zhong and Y. Hu, *J. Power Sources*, 2022, **545**, 231908.
23 L. Yan, B. B. Xie, C. Yang, Y. H. Wang, J. Q. Ning, Y. J. Zhong and Y. Hu, *Adv. Energy Mater.*, 2023, **13**, 2204245.
24 X. H. Chen, K. Niu, Z. Y. Xue, X. D. Liu, B. G. Liu, B. Zhang, H. Zeng, W. Lv, Y. M. Zhang and Y. Wu, *Nanoscale Adv.*, 2022, **4**, 1639–1648.
25 B. He, P. Zhao, G. X. Pan, Q. Lu, H. Q. Li, F. Ye, Y. W. Tang, Q. L. Hao and Z. Su, *J. Alloys Compd.*, 2023, **938**, 168673.
26 Y. K. Sun, W. Y. Sun, G. C. Li, L. Wang, J. F. Huang, A. Meng and Z. J. Li, *J. Mater. Chem. A*, 2023, **11**, 2262–2272.
27 L. Yan, Z. Y. Xu, X. N. Liu, S. Mahmood, J. L. Shen, J. Q. Ning, S. Li, Y. J. Zhong and Y. Hu, *Chem. Eng. J.*, 2022, **446**, 137049.
28 H. Y. Wang, Y. K. Jiao, S. J. Wang, P. C. Ye, J. Q. Ning, Y. J. Zhong and Y. Hu, *Small*, 2021, **17**, 2103517.